Regulatory Toxicology and Pharmacology 109 (2019) 104489

Contents lists available at ScienceDirect

Regulatory Toxicology and Pharmacology

journal homepage: www.elsevier.com/locate/yrtph

# Antineoplastic properties of zafirlukast against hepatocellular carcinoma via activation of mitochondrial mediated apoptosis

Pranesh Kumar[a,1], Aakriti Agarwal[a,1], Ashok K. Singh[a], Anurag Kumar Gautam[a], Sreemoyee Chakraborti[b], Umesh Kumar[b], Dinesh Kumar[b], Bolay Bhattacharya[c], Parthasarathi Panda[d], Biswajit Saha[e], Tabish Qidwai[f], Biswanath Maity[b], Sudipta Saha[a,*]

[a] Department of Pharmaceutical Sciences, Babasaheb Bhimrao Ambedkar University, Vidya Vihar, Raibareli Road, Lucknow, 226025, India
[b] Centre of Biomedical Research, SGPGIMS Campus, Raebareli Road, Lucknow, 226014, Uttar Pradesh, India
[c] Gethanjali College of Pharmacy, Cheeryal, Keesara, Hyderabad, 501301, India
[d] Dr. B.C. Roy College of Pharmacy & Allied Health Sciences, Dr. Meghnad Saha Sarani, Bidhan Nagar, Durgapur, 713206, WB, India
[e] Department of Chemical Engineering, National Institute of Technology, Rourkela, Odisha, 769008, India
[f] Faculty of Biotechnology, IBST, Shri Ramswaroop Memorial University Lucknow, Deva Road, UP, 225003, India

ARTICLE INFO

*Keywords:*
Zafirlukast
Hepatocellular carcinoma
Bcl-2 and BAX proteins
Apoptosis
$^{1}$H-NMR based metabolomics

ABSTRACT

Hepatocellular carcinoma (HCC) is one of the most common cancers worldwideand haslimited treatment options. In view of this, zafirlukast (ZAF) was administered orally to DEN-induced HCC rats to evaluate its antineoplastic properties. ELISA, qRT-PCR and Western blot were used to determine the molecular mechanism associated with ZAF therapy for HCC. We found that HCC developed as a result of lower expression of caspases 3 and 9, but their levels returned to normal when the expression of eNOS, BAX, BAD, and Cyt C was decreased and when the expression of iNOS, Bcl-xl, and Bcl-2 was increased. Again, ZAF (80 mg/kg dose) treatment normalized the expression of caspase-mediated apoptotic factors, i.e. BAX and Bcl-2 proteins, as established through Western blot analysis. Later, $^{1}$H NMR-based serum metabolomics study revealed that levels of perturbed metabolites in DEN-induced rat serum returned to normal after ZAF administration. Altogether, the antineoplastic potential of ZAF was found to be comparable, and to some degree better, than the marketed chemotherapeutic 5-flurouracil, which may be beneficial for anti-HCC treatment from a future drug design perspective.

## 1. Introduction

HCC is the fifth and seventh most common cause of cancer in men and women, respectively, and is the third most common cause of cancer-related death worldwide (Ferlay et al., 2010; Lin et al., 2016). The molecular mechanisms of HCC are still unknown, and thus medical doctors are challenged as the demand for HCC treatment increases each day. Synthetic chemotherapeutic agents have been shown to have good efficacy for HCC treatment, but researchers have achieved very little success due to chemo-resistance (Keshari et al., 2017). Sorafenib is the only drug of choice for HCC treatment, but it has a poor efficacy with possibility of resistance (Park, 2015; Wilhelm et al., 2006). Therefore, it is necessary to explore some newer anticancer drugs to prolong the survival of patients with HCC.

A previous literature review suggested that zafirlukast (ZAF) is used to cure asthma via agonistic action on cysteinyl leukotriene receptor-1 (CysLT1) (Kahnt et al., 2013). CysLT1 triggers colitis-associated colon cancer in a mouse model (Osman et al., 2017), and a CysLT1 antagonist, montelukast, inhibited tumor growth in a xenograft mouse model of colon cancer (Savari et al., 2013). Therefore, we questioned whether ZAF exerts antineoplastic effects since it is structurally similar to montelukast and has a similar mechanism of action, i.e. CysLT1 antagonistic properties. Before performing an *in vivo* study, we investigated the anti-HCC potential of ZAF using a human liver cancer cell line (Hep-G2 cells) and demonstrated its strong antiproliferative potential against Hep-G2 cells ($IC_{50}$ ~13.95 μM) (Supplementary Data Sheet, Fig. S1). Inspired by the aforementioned finding, we speculated that ZAF might be an effective agent for the treatment of HCC.

An earlier report documented that oxidative stress and liver injury have important roles in HCC development and that the carcinogenic action of diethylnitrosamine (DEN) has a specific role in inflammation and oxidative stress in liver tissue (Kumar et al., 2015). Therefore, to

* Corresponding author. Department of Pharmaceutical Sciences, Babasaheb Bhimrao Ambedkar University, Vidya Vihar, Raebareli Road, Lucknow, 226025, India.
*E-mail address:* sudiptapharm@gmail.com (S. Saha).
[1] All the authors contributed equally.

https://doi.org/10.1016/j.yrtph.2019.104489
Received 28 March 2019; Received in revised form 1 October 2019; Accepted 3 October 2019
Available online 09 October 2019
0273-2300/ 

evaluate the molecular mechanism of the anti-HCC potential of ZAF, we performed an *in vivo* experiment using a DEN-induced HCC rat model. Various apoptotic (caspases-3 and 9) and inflammatory (IL-2, IL-6, IL-10 and IL-1β) mediators in liver tissues were analyzed through enzyme linked immunosorbent assay (ELISA). Apoptotic markers exhibited promising effects as compared with inflammatory mediators, and thus, we decided to perform a mechanistic study on apoptotic pathways using gene and protein expression analyses at the molecular level. Later, a proton nuclear magnetic resonance ($^1$H-NMR)-based serum metabolomics study was performed to differentiate the metabolic perturbations associated with HCC before and after ZAF treatment.

## 2. Materials and methods

### 2.1. Drugs and reagents

All chemicals were purchased from Sigma-Aldrich, Bangalore and Loba Chemicals, New Delhi, India. The chemicals used in qRT-PCR and Western blot were procured from Genetix Biotech Asia Pvt. Ltd., New Delhi, and Thermo-Fisher Scientific, Bangalore, India. All the solvents and chemicals were analytical grade with 99% purity; in-house distilled water was used for all experiments.

### 2.2. Experimental design

Male albino Wistar rats (100–120 g) were used for this experiment (Approval No 1648/PO/Re/S/12/CPCSEA/54). Animals were acclimatized to laboratory conditions (temperature [25 ± 1 °C] with a light/dark cycle of 12 h and had ad libitum access to a commercial pellet diet and water)for one week before the experiment. Six-week-old experimental Wistar albino rats were randomly allocated to 5 groups with 8 animals in each group (n = 8). The groups were classified as follows: Group 1 (Normal Control, NC): 0.25% CMC (2 mL/kg), Group 2(Carcinogen Control, CC): N-nitrosodiethylamine (DEN, 100 mg/kg, i. p. once a week for 6 weeks) (Matsuzaki et al., 1992), Group 3 (Positive Control, PC): DEN + 5-FU (10 mg/kg, i. p. for 15 days after HCC induction), Group 4: DEN + ZAF(T1, 40 mg/kg, orally for 15 days after HCC induction), and Group 5: DEN + ZAF(T2, 80 mg/kg, orally for 15 days after HCC induction) (Mahgoub et al., 2003).

Recent reports have documented that HCC is induced in Wistar albino rats by i. p. injection of DEN at a dose of 100 mg/kg body weight once a week for 6 weeks (Matsuzaki et al., 1992). By adopting this protocol, DEN was administrated to all animals in groups 2 to 5 after they had adapted to experimental conditions in the first week. Six weeks later, after the completion of DEN administration, 5-FU, T1 and T2 were given to the animals for 15 days as a curative agent against hepatic injury. The dose given to rats in the T1 and T2 groups, i.e. the dose of ZAF, was selected according to previously published literature (Mahgoub et al., 2003). At the end of treatment, the animals were sacrificed by cervical dislocation after which the livers were immediately excised, rinsed in ice-cold saline and stored at −80 °C for further oxidative parameter analysis and for exploration of gene and protein expression at the molecular level. A portion of the tissues were stored in 10% formalin for further histopathological studies.

### 2.3. Estimation of various physiological and biochemical parameters

Body weight changes were measured on the initial and final days of the experiment and % weight gains were calculated at the later stage. The number of carcinogenic nodules and their % incidence were also calculated to observe the cytotoxic effects between treated and untreated groups. On the contrary, the levels of oxidative stress parameters such as protein carbonyl (ProC), thiobarbituric acid reactive substances (TBARS), glutathione (GSH), superoxide dismutase (SOD) and catalase (CAT) (Sahdev et al., 2017; Yadav et al., 2015; Singh et al., 2018a, 2018b; Kumar et al., 2017) were estimated in liver tissue. Serum lipid profiles such as those of total cholesterol (TC) (ADL/V.02/110314), triglycerides (TG) (ADL/V.02/110314) and high-density lipoprotein (HDL) (ADL/V.02/180114) were estimated using a lipid profile kit (Agappe Diagnostic Ltd., Kerala, India). Low-density lipoprotein (LDL) and very low-density lipoprotein (VLDL) were estimated using Friedewald's formula (Singh et al., 2018b), [LDL (mg/dL) = TC – HDL – (TG/5); VLDL (mg/dL) = TC – HDL – LDL]. The serum levels of enzymes such as alanine aminotransferase (ALT) (4-FBCER-GPT), alkaline phosphatase (ALP) (DALP-250), aspartate aminotransferase (AST) (4-FBCER-GOT), and lactate dehydrogenase (LDH) (11407001) (Sahdev et al., 2017) were estimated using commercially available kits. The procedures adopted for determination of catabolic by-products (bilirubin and biliverdin) in liver tissue have been previously described (Singh et al., 2018a; Kumar et al., 2017).

### 2.4. GSH/GSSG assay

The GSH/GSSG assay was performed to analyze the ratio of GSH to GSSG in liver tissue. The detailed procedure was adopted per the instructions provided in the GSH and GSSG Assay Kit (K261-100, BioVision, Mountain View, USA). The levels of GSH and GSSG were measured using a fluorescence microplate reader (Biotek Instrument Inc., Winooski, VT, USA) at Ex/Em wavelengths of 340/420 nm.

### 2.5. Histopathology and SEM of liver tissue

Histopathological studies were also performed to determine the tissue and intracellular configuration changes of liver cells after ZAF administration. Liver tissues from each group were assessed for morphological changes using hematoxylin and eosin staining. The tissues were preserved in 10% formalin overnight. The next day, the cells were again soaked in 70% isopropanol overnight. Later, the tissues were exposed to isopropanol at various concentrations (70, 90, and 100%) and dehydrated in 100% xylene. The tissue samples were then embedded in bees wax, and sections 5 μm in thickness were prepared using a microtome. Finally, the tissues were stained with hematoxylin and eosin and observed under a microscope (magnification 40X).

For SEM analysis, liver tissue samples were collected (sections 2–4 mm in thickness) and fixed in 2.5% glutaraldehyde for 2–6 h at 4 °C for primary fixation. Then, the samples were washed with 0.1 M phosphate buffer for 15 min at 4 °C. Next, 1% osmium tetroxide was used for post-fixation for 2 h at 4 °C. The samples were again washed in 0.1 M phosphate buffer three times for 15min each time and were maintained at 4 °C. Later, these samples were dehydrated in anhydrous acetone, and all specimens were air dried at room temperature and coated with platinum using critical point drying (31.5 °C at 1100 psi). Finally, samples were mounted on to aluminum stubs with adhesive tape and were examined for morphological changes using SEM (JEOL JSM-6490LV) (Singh et al., 2018a).

### 2.6. Estimation of cytokines by ELISA

Elevated levels of pro-inflammatory cytokines such as IL-2 (RAB0288) and IL-6 (RAB0311) were detected using ELISA kits obtained from Sigma Aldrich, Bengaluru, India. ELISA kits for other cytokines such as IL-10 (GX-8140E1) and IL-1β (GX-3930-E1) were obtained from Gemetix Biotech Asia Pvt. Ltd., New Delhi, India. The levels of caspase-3 (KHO1091) and caspase-9 (ITER0804) were detected using kits purchased from Invitrogen Bioservices India Pvt. Ltd. (Thermo Fisher), Bengaluru, India and Geno Technology Inc., Noida, India (Singh et al., 2018a).

### 2.7. Quantitative real-time polymerase chain reaction (qRT-PCR) analysis

Ten mg of hepatic tissue from each group was placed into 1.5 mL microcentrifuge tubes followed by the addition of TRIzol reagent to

isolate RNA. An RNeasy mini kit was used to purify the mRNA. The mRNA concentrationwas estimated using a Nano Drop instrument at 260/280 nm cDNA was then prepared according to the manufacturer's protocol for the GeneSure first strand cDNA synthesis kit (Genetix Biotech Asia Pvt. Ltd., New Delhi, India). Finally, qRT-PCR was performed in an Agilent Stratagene Mx3000P series (Applied Biosystems, Foster City, USA) using Sybr® green PCR master mix. The cDNA was denatured at 94 °C for 5 min and annealed at 58 °C for 30 s and further elongation was performed at 72 °C for 35 s. Forty cycles were used forqRT-PCR, which helped in the detection of amplified DNA in real-time. The mRNA was normalized to the housekeeping control β-actin. ΔCt and $2^{-\Delta\Delta Ct}$ were calculated according to a previously described procedure (Singh et al., 2018a, 2018b; Kumar et al., 2017). The primer sequences were as follows:β-actin, 5′-AAGTCCCTCACCCTCCCAAAAG-3′ (forward) 5′- AAGCAATGCTGTCACCTTCCC-3′ (reverse) (Singh et al., 2018a), caspase-3, 5′-GGTATTGAGACAGACAGTGG-3′ (forward) and 5′-CATGGGATCTGTTTCTTTGC-3′ (reverse) (Kumar et al., 2018); and caspase 9, 5′-AGTTCCCGGGTGCTGTCTAT-3′ (forward) and 5′-GCCAT GGTCTTTCTGCTCAC-3′ (reverse) (Xu et al., 2016). iNOS, 5′-GTGCTA ATGCGGAAGGTCATG-3′ (forward), 5′-GCTTCCGACTTTCCTGTCTCA GTA-3′ (reverse); eNOS, 5′- CGGCATCACCAGGAAGAA.

GA-3′ (forward), 5′-CATGAGCGAGGCGGAGAT-3′ (reverse) (Anadol et al., 2012); Cytochrome C, 5′-TTTGGATCCAATGGGTGATGTTGAG-3′ (forward), 5′-TTTGAATTCCTCATTAGTAGCTTTTTTGAG-3′ (reverse) (Chandra et al., 2002); Bcl-2, 5′-CTGGTGGACAACATCGCTCTG-3′ (forward) 5′-GGTCTGCTGACCTCACTTGTG-3′ (reverse) (Jafari et al., 2008); Bcl-xl, 5′ AGGCTGGCGATGAGTTTGAA-3′ (forward), 5′-TGAAA CGCTCCTGGCCTTTC-3′ (reverse) (Jafari et al., 2008); BAX, 5′-TTCAT CCAGGATCGAGCAGA-3' (forward) 5′-GCAAAGTAGAAGGCAACG-3' (reverse) (Jafari et al., 2008); BAD, 5′-CTCCGAAGAATGAGCGATGAA-3' (Forward) 5′-ATCCCACCAGGACTGGATAA-3' (Reverse) (Jafari et al., 2008).

### 2.8. Western blot analysis

The protein expression levels of Bcl-2, and BAX were assessed by immunoblotting. All antibodies were purchased from Thermo Fisher Scientific (Waltham, MA, USA). Radioimmunoprecipitation assay (RIPA) buffer was used to lyse the cells, which were centrifuged at 10,000 rpm for 15 min at 4 °C; Bradford reagent was used to estimate protein concentrations. Proteins (50 μg) were electrophoresed on 12% sodium dodecyl sulfate (SDS)-polyacrylamide gel and immediately transferred to a polyvinylidene fluoride membrane. The membranes were blocked in 5% skimmed milk containing phosphate-buffered saline (PBS) with 0.1% Tween-20 (PBS-T) for 3 h at 4 °C and probed overnight at 4 °C with the following primary antibodies (obtained from Cell Signaling Technology, MA, USA) diluted in PBS-T: Bcl-2, BAX, and a tubulin rabbit monoclonal antibody (1:500 dilution for each). The following day, the membranes were washed three times with tris-buffered saline containing Tween-20 (TBS-T) and incubated with anti-rabbit secondary antibodies linked to horse-radish peroxidase at a 1:3000 dilution at room temperature for 3 h. The film was washed three times with TBST, and the membrane was developed with enhanced chemiluminescence ECL (Pierce™ ECL Western Blotting Substrate); images were obtained using Chemidoc (Clinx Scientific Instruments, China) (Han et al., 2016; Sui et al., 2011).

### 2.9. $^1$H-NMR-based metabolomic studies

All samples were prepared according to a previously described procedure (Sahdev et al., 2017). NMR spectra were recorded at 298 K using a Bruker BiospinAvance-III 800 MHz NMR spectrometer (equipped with Cryoprobe) set at a proton frequency of 800.21 MHz. In all, 400 μL of serum was transferred to a 5 mm NMR sealed tube, and a sealed capillary tube containing a known concentration of TSP was inserted separately for the purpose of locking and chemical shift referencing. For each serum sample, transverse relaxation-edited CPMG (Carr–Purcell–Meiboom–Gill) NMR spectra were acquired using the standard Bruker's pulse program library sequence (CPMGPR1D) with pre-saturation of the water peak, which was achieved by irradiating it continuously during the recycle delay (RD) of 5 s.

For the assignment of various peaks in the 1D $^1$H-CPMG NMR spectra, chemical shifts were identified and assigned by comparing the chemical shifts using the database library of Chenomax 8.1 software NMR suite (Chenomx Inc., Edmonton, Canada). The remaining peaks in the CPMG $^1$H-NMR spectra were assigned by adopting the previously reported NMR spectra of metabolites as well as data obtained from the HMDB (Human Metabolome Database) (Wishart et al., 2007) and BMRB (Biological Magnetic Resonance Data Bank) (Ulrich et al., 2007).

The multivariate data analysis was performed using $^1$H-CPMG. Before the data analysis, all the $^1$H-NMR spectra were manually phased and baseline-corrected using TopSpin3.0 (Bruker NMR data Processing Software). For the multivariate analysis, the CPMG (δ 8.5–0.5) ppm spectra were binned and integrated automatically using AMIX package (Version 3.8.7, Bruker, BioSpin). The binned data from CPMG experiments were subjected to chemometrics data analysis using the web-based tools server MetaboAnalyst(version 3.0; freely available web-server for academic use: https://www.metaboanalyst.ca/) (Xia et al., 2009, 2015).

Principal component analysis (unsupervised approach) was first performed to identify the outliers. To further demonstrate the differences between the different groups, supervised partial least squares discriminate analysis with orthogonal signal correction (OPLS-DA) was performed to expose class separations between the groups and to identify the metabolites significantly contributing to group differentiation. The validations of the OPLS-DA models were measured through $R^2$ and $Q^2$ in PLS-DA models. The PLS-DA model was further used to identify the metabolites responsible for the discrimination based on their higher values of variable significance on projection scores (i.e. VIPs) and showing statistical significance as estimated based on a 0.05 level of probability, i.e. a p-value $< 0.05$ (calculated using the Mann-Whitney test for pairwise comparisons). The box plot representation and area under the curve (AUC) were measured by univariate analysis. This was related to visualizing the variation in the levels of significantly altered metabolites as well as the discriminatory ability of metabolites, as shown bypotential biomarkers, with values close to 1 as a better classification. Moreover, a *t*-test univariate analysis was employed to determine the significance biomarker of the variable (*p*-value) along with the up and down regulation of metabolites.

### 2.10. Statistical data analysis

Statistical data analysis was performed using GraphPad Prism 5.0 (San Diego, CA, USA). The results were expressed as the mean ± standard deviation (SD) (n = 8). The statistical data were analyzed by one-way ANOVA (analysis of variance) followed by Bonferroni's multiple comparison test. Statistically significant differences were observed between carcinogen control (CC) and test groups [one way-ANOVA followed by Bonferroni multiple comparison test (***$p < 0.001$, **$p < 0.01$,*$p < 0.05$)].

## 3. Results

### 3.1. Evaluation of physiological and biochemical parameters, catabolic by-products in the liver and various enzyme levels in the serum

Various physiological parameters (body and liver weights, tumor incidence) were improved after oral ZAF administration (Table 1). It is obvious from the data that the DEN-treated groups experienced a major loss in body weight and improved condition after ZAF treatment, particularly at the 80 mg/kg dose. Similar trends were found for liver weight and tumor incidence (Table 1).

**Table 1**
Study of zafirlukast treatment on the liver parameters in NDEA-exposed carcinogenesis in rats. (NC: Normal Control, CC: Carcinogen Control, PC: Positive Control, **T1:** zafirlukast (40 mg/kg) and **T2:** zafirlukast (80 mg/kg).

| Sr.No. | Groups | Initial day body weight (g) | Final day body weight (g) | Weight variation (g) | Liver weight (g) | Tumor incidence no. |
|---|---|---|---|---|---|---|
| 1 | NC | 135.00 ± 2.16 | 155.00 ± 2.43 | 20.00 ± 0.97 | 3.72 ± 0.21 | 0.00 ± 0.00 |
| 2 | CC | 141.00 ± 1.82 | 107.00 ± 5.18 | −34.00 ± 2.24 | 7.29 ± 0.94 | 31.00 ± 2.54 |
| 3 | PC | 146.00 ± 2.79 | 154.00 ± 2.78*** | 8.00 ± 1.02*** | 4.52 ± 0.64*** | 15.00 ± 1.42*** |
| 4 | **T1** | 126.00 ± 3.19 | 132.00 ± 3.85*** | 6.00 ± 0.82*** | 5.84 ± 1.06** | 18.00 ± 0.87*** |
| 5 | **T2** | 135.00 ± 2.15 | 151.00 ± 3.15*** | 16.00 ± 1.97*** | 4.11 ± 0.81*** | 12.00 ± 1.07*** |

Data represented here as mean ± SD (n = 8). Statistically significant differences were observed between CC and test groups [one way ANOVA followed by Bonferroni multiple comparison test (***p < 0.001, **p < 0.01 and *p < 0.05)].

**Table 2**
Study of anti-oxidative parameters in NDEA-exposed carcinogenesis in rats. (NC: Normal Control, CC: Carcinogen Control, PC: Positive Control, **T1:** zafirlukast (40 mg/kg) and **T2:** zafirlukast (80 mg/kg).

| Sr.No. | Parameters | NC | CC | PC | T1 | T2 |
|---|---|---|---|---|---|---|
| 1. | SOD (U/μg of protein) | 1.45 ± 0.07 | 0.83 ± 0.04 | 1.27 ± 0.05*** | 0.97 ± 0.08*** | 1.25 ± 0.04*** |
| 2. | CAT (nM of $H_2O_2$/min/μg of protein) | 5.10 ± 0.86 | 0.40 ± 0.26 | 3.96 ± 0.08*** | 2.93 ± 0.03*** | 2.99 ± 0.06*** |
| 3. | PC (μM/μg of protein) | 0.08 ± 0.002 | 0.21 ± 0.01 | 0.10 ± 0.01*** | 0.18 ± 0.03 | 0.10 ± 0.04*** |
| 4. | TBARS (nM of MDA/mg of protein) | 64.08 ± 3.25 | 94.65 ± 3.01 | 68.50 ± 3.40*** | 70.03 ± 2.32*** | 66.13 ± 2.09*** |
| 5. | GSH (μM/μg of protein) | 8.81 ± 0.79 | 5.60 ± 0.47 | 8.85 ± 0.67*** | 6.21 ± 1.06 | 8.23 ± 0.42*** |
| 6. | GSH/GSSG ratio | 15.67 ± 0.89 | 9.76 ± 0.52 | 15.43 ± 0.95*** | 13.01 ± 1.13*** | 15.28 ± 0.84*** |

Data represented here as mean ± SD (n = 8). Statistically significant differences were observed between CC and test groups [one way ANOVA followed by Bonferroni multiple comparison test (***p < 0.001, **p < 0.01 and *p < 0.05)].

In the later stage, various oxidative stress parameters were measured in liver tissue to evaluate the antioxidant properties of ZAF. In HCC rats treated with DEN, SOD, CAT and GSH concentrations were decreased, while those of MDA and ProC were increased (CC group, Table 2). An approximate 40 and 90% reduction was observed in SOD and CAT, respectively, in the CC group compared with the NC group. Improvements in SOD and CAT levels were observed after treatment with ZAF, particularly at the 80 mg/kg dose, which was comparable with the positive control, i.e. the 5-FU-treated group. Similar trends were found for GSH measurements, as we observed a reduction in its concentration in the CC group (~5.60 μM) compared with the NC group (~8.81 μM). Treatment with ZAF significantly normalized the GSH concentration to a normal level (Table 2). In addition, the production of MDA and ProC was measured in a similar experiment. MDA production was almost 1.5 times higher in the CC (~94.65 nM) than in the NC group (~64.08 nM). However, treatment with ZAF at two doses (~66.13 nM) attenuated MDA formation. A similar trend was noted in the ProC level, which had an approximately 2.5 times higher attenuation in CC rats. Treatment with ZAF significantly normalized the ProC level as shown in Table 2.

Regarding the serum lipid profiles, TC, TG, LDL and VLDL, but not HDL, were increased in the CC group compared with the NC group. Both TC and TG levels were normalized after oral administration of ZAF. In addition, both LDL and VLDL were improved up to 50% after ZAF treatment (Table 3). In contrast, HDL levels were dramatically decreased in CC rats (~29.74 mg/dL) compared with NC rats (~47.27 mg/dL). The HDL concentration in the serum improved to normal levels after the oral administration of both doses of ZAF (Table 3).

AST, ALT, LDH, and ALP in the serum were measured in a similar fashion to evaluate the protective effect of ZAF (Fig. 1A). CC rats showed a significant increase in all these enzymes compared with NC rats. The oral administration of ZAF at both doses attenuated the levels of all these enzymes ($p < 0.001$) compared with what was observed in the CC rats. Furthermore, the effects of ZAF on the generation of catabolic pigments (bilirubin and biliverdin) in liver tissues were also analyzed (Fig. 1B). ZAF treatment normalized these catabolic by-products to more normal levels, as they were elevated more than 1.5-fold in the CC group. The higher dose of ZAF, i.e. 80 mg/kg, was similar to that of 5-FU (standard chemotherapeutic).

### *3.2. Effect of ZAF on the GSH/GSSG ratio, a potential oxidative stress marker*

GSH (glutathione), which is the most abundant thiol-containing peptide antioxidant in mammals, neutralizes free radicals after being oxidized to glutathione disulfide (GSSG). Particularly in the ZAF-treated group, an increased GSH/GSSG ratio was observed, which indicated that ZAF has antioxidant property.

**Table 3**
Lipid profiles in serum to evaluate the ameliorative effects after DEN and (zafirlukast) administration, (NC: Normal Control, CC: Carcinogen Control, PC: Positive Control, **T1:** zafirlukast (40 mg/kg) and **T2:** zafirlukast (80 mg/kg).

| Sr.No. | Parameters | NC | CC | PC | T1 | T2 |
|---|---|---|---|---|---|---|
| 1. | TC (mg/dL) | 120.13 ± 2.71 | 151.41 ± 2.45 | 131.85 ± 2.01*** | 135.57 ± 5.40*** | 127.59 ± 4.99*** |
| 2. | TG (mg/dL) | 68.50 ± 2.35 | 132.32 ± 4.59 | 77.61 ± 2.37*** | 81.04 ± 4.80*** | 70.71 ± 2.03*** |
| 3. | HDL (mg/dL) | 47.27 ± 1.59 | 29.74 ± 0.84 | 41.32 ± 2.07*** | 36.26 ± 4.38*** | 43.94 ± 4.06*** |
| 4. | LDL (mg/dL) | 59.16 ± 0.65 | 95.21 ± 0.69 | 75.01 ± 0.41*** | 83.10 ± 0.20*** | 69.52 ± 0.38*** |
| 5. | VLDL (mg/dL) | 13.70 ± 0.47 | 26.47 ± 0.92 | 15.51 ± 0.35*** | 16.20 ± 0.96*** | 14.14 ± 0.41*** |

Data represented here as mean ± SD (n = 8). Statistically significant differences were observed between CC and test groups [one way ANOVA followed by Bonferroni multiple comparison test (***p < 0.001, **p < 0.01 and *p < 0.05)].

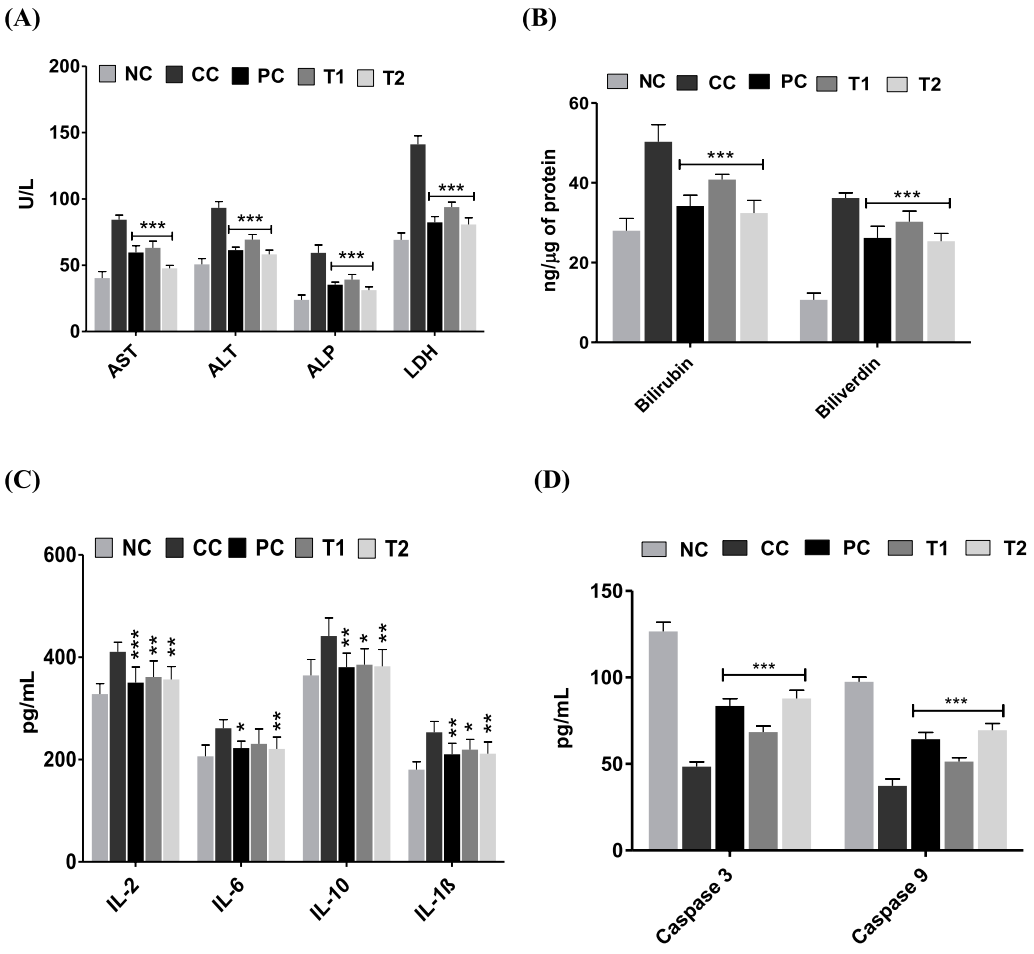


**Fig. 1.** Effects of zafirlukast after oral administration of 40 mg/kg and 80 mg/kg for 15 days in carcinogen control rats **(A)** Enzyme levels of AST, ALT, CPK and LDH in serum, **(B)** Catabolic by-product (bilirubin and biliverdin), and **(C)** Anti-proliferative biomarkers IL-2, IL-6, IL-10, IL-1β, **(D)** Caspase 3 and caspase 9. Data are represented as mean ± SD (n = 8). Statistically significant differences were observed between carcinogen control and test groups [one way-ANOVA followed by Bonferroni multiple comparison test (***p < 0.001, **p < 0.01, *p < 0.05)]. The studied groups are: (NC: Normal Control, CC: Carcinogen Control, PC: Positive Control, **T1:** zafirlukast (40 mg/kg) and **T2:** zafirlukast (80 mg/kg).

### *3.3. ELISA determination of various pro-inflammatory and apoptotic mediators*

To assess the antineoplastic potential of ZAF on cancer-mediated inflammatory and apoptotic markers, enzyme linked immunosorbent assays (ELISAs) were performed to predict the concentrations of pro-inflammatory cytokines (IL-2, IL-6, IL-10 and IL-1β) (Fig. 1C) and apoptotic mediators (Caspase-3 and 9) in the rat liver (Fig. 1D). Significant differences were not documented in pro-inflammatory cytokines between the groups. However, the levels of apoptotic markers were reduced ~2.5-fold in CC rats compared with NC rats. ZAF treatment significantly restored the concentrations of caspase-3 and 9, and a more pronounced effect was observed at the 80 mg/kg dose, which was comparable with the dose of 5-FU.

### *3.4. Histopathology of liver tissue*

Again, hematoxylin and eosin (H & E) staining was used to determine the tissue and intracellular configuration changes in the livers of rats in various groups. In the NC group, normal architecture of Kupffer cells (K) with abundant nuclei was observed during histopathological examination. However, the liver cells of the CC group had lost their normal cellular architecture, and specifically, the carcinogenic livers contained more pronounced ruptured hepatic cells (RC), irregular sinusoids, tumor anaplastic cells (TA), degenerated nuclei (dN) in K cells and tumoral vacuoles (Fig. 2). A marked improvement in gross microscopic appearance of hepatic tissue was observed after the treatments (Fig. 2).

### *3.5. qRT-PCR and Western blot analyses*

We performed qRT-PCR analysis to measure the gene expression levels of iNOS, eNOS, BAX, BAD, Bcl-2, Bcl-xl, Cyt C, and caspases 3 and 9. The analysis revealed upstream regulation of the iNOS, Bcl-2, and Bcl-xl and downstream regulation of eNOS, BAX and BAD, caspases 3 and 9, and Cyt C genes in the CC group compared with the NC group. Administration of 5-FU and ZAF normalized all these upstream- and downstream-regulated genes (Fig. 3A). The potency of ZAF at 80 mg/kg was found to be comparable and to some degree better than that of the chemotherapeutic currently available on the market (5-FU).

On the contrary, a quantitative Western blot analysis was used to measure the protein expression levels of BAX and Bcl-2. The levels of BAX protein were down regulated in CC rats with respect to NC rats and again improved after the administration of a higher dose of ZAF (Fig. 3B–D). An opposite trend was noted for Bcl-2, which was up-regulated in CC rats and became normalized after ZAF treatment. Tubulin served as a housekeeping protein in this experiment (Supplementary Data Sheet, Fig. S2).

### *3.6. $^{1}$H-NMR-based metabolomics to assess the biochemical impact of ZAF treatment*

The individual 1D $^{1}$H-CPMG NMR spectra acquired from serum samples from different control and treated rats, with the assigned resonances, are shown in Figs. 4–6. The $^{1}$H-NMR spectra of serum samples showed signals primarily from lipids/lipoproteins [(e.g. low density lipoprotein (LDL), very low density lipoprotein (VLDL), Poly-unsaturated fatty acids (PUFAs etc.)], membrane metabolites [(e.g.

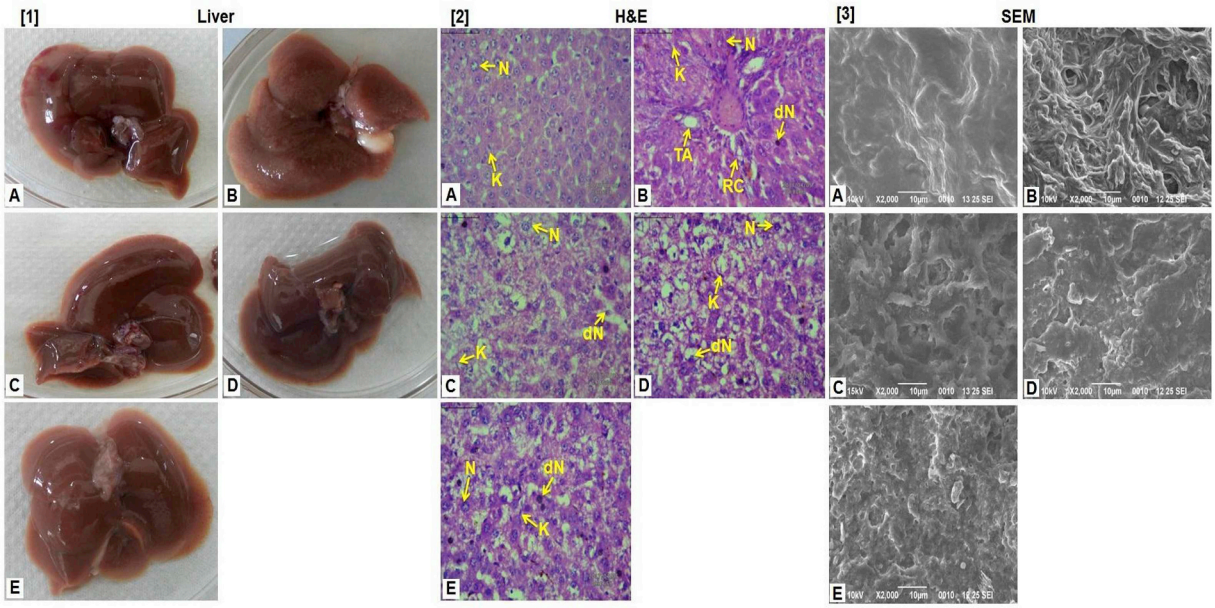


**Fig. 2.** The hepatic pathological changes in DEN-induced rats. **[1]** Intact Liver: showing numerous carcinogenic nodules in carcinogen control group that were reduced significantly or absent after treatments with 5-FU, zafirlukast (40 mg/kg and 80 mg/kg), **[2]** Histopathological changes (40X, Scale bar 50 μm). The abbreviations used are: Normal nucleus (N), degenerated nucleus (dN), ruptured hepatic cells (RC), Tumor anaplastic cells (TA). **[3]** Scanning Electron Microscopic photomicrographs of the liver tissues (2000X) and the studied groups are: (**A**: Normal Control, **B**: Carcinogen Control, **C**: Positive Control, **D:** zafirlukast (40 mg/kg) and **E:** zafirlukast (80 mg/kg).

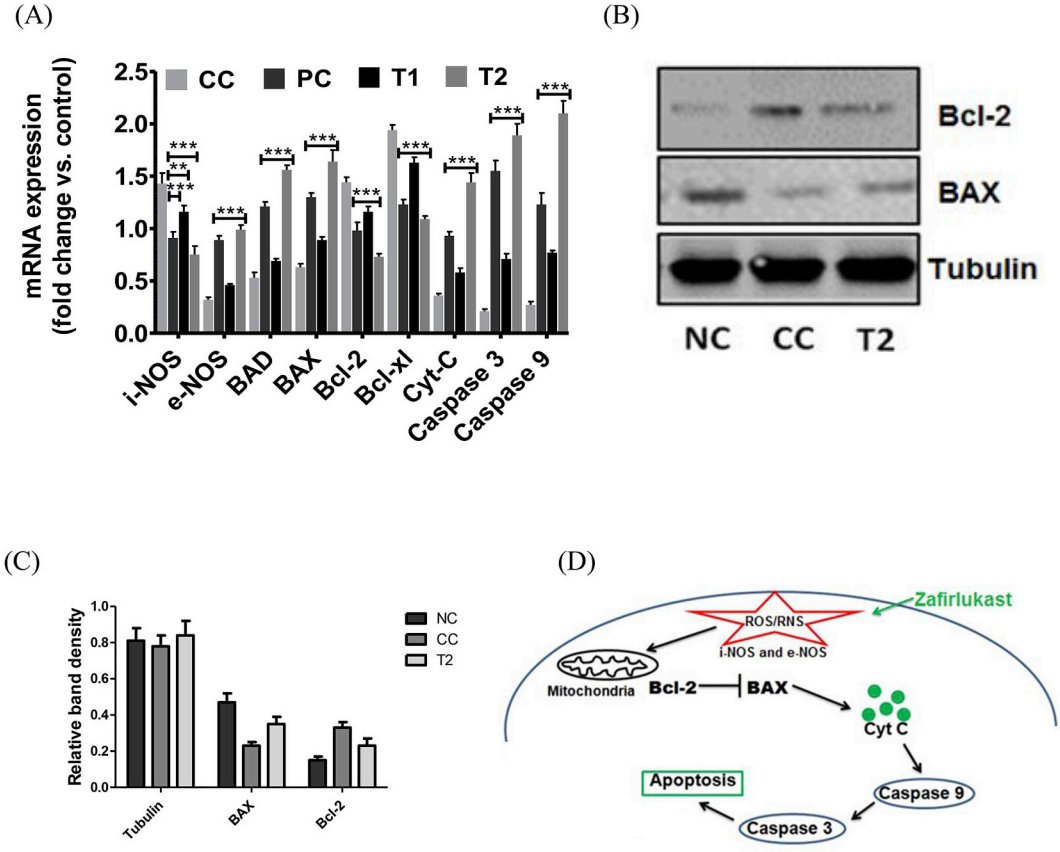


**Fig. 3. (A)** Gene expression levels of i-NOS, e-NOS, BAD, BAX, Bcl-2, Bcl-xl, Cyt-C, caspase-3 and caspase-9 in liver tissue, **(B)** Protein expression levels of BAX, Bcl-2 and tubulin in liver tissue after treatment with zafirlukast (determined by quantitative Western blot analysis), **(C)** Plausible mechanism of anticancer activity of zafirlukast. Data are represented as mean ± SD (n = 8). Statistically significant differences were observed between carcinogen control and test groups [one way-ANOVA followed by Bonferroni multiple comparison test (***p < 0.001, **p < 0.01, *p < 0.05)]. The studied groups are: (NC: Normal Control, CC: Carcinogen Control, PC: Positive Control, **T1:** zafirlukast (40 mg/kg) and **T2:** zafirlukast (80 mg/kg).

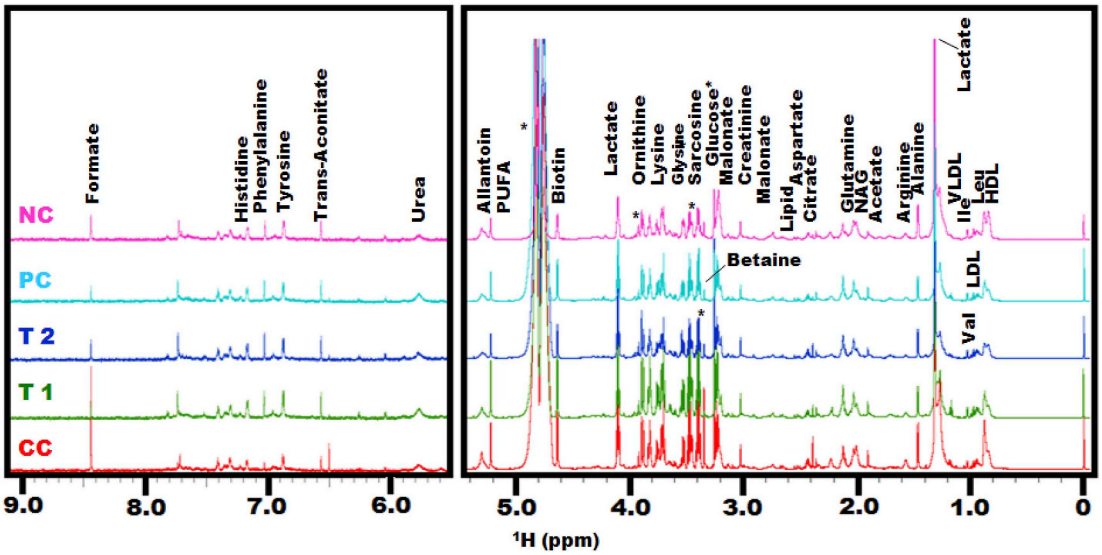


**Fig. 4.** Stack plot of representative 1D $^{1}$H CPMG NMR spectra of rat serum obtained from different groups. Carcinogen control (CC), Treatment low dose (T1) & Treatment high dose (T2), Positive control (PC), Normal Control (NC) groups.

choline], N-acetyl and O-acetyl glycoproteins (NAG, OAG), and amino acids [(e.g. leucine, tyrosine etc.)]. Other identified metabolites were, glucose, lactate, acetate, citrate, creatine, formate, glycerol and trans-aconitate (Figs. 4–6).

Further, the $^{1}$H-NMR dataset was subjected to statistical data modelling and analysisusing multivariate analysis tools in MetaboAnalyst (Xia et al., 2009, 2015). First, a PCA model was employed to authenticate the analytical quality system performance and to observe possible outliers. An OPLS-DA model was then used to obtain a summary of the complete dataset of the samples and to discriminate the variables that are responsible for variations among the groups. The quality of the OPLS-DA model was optimized with two variables: $Q^2$ and $R^2$. Score plots obtained from the 1D $^{1}$H CPMG NMR spectra (Fig. 4) (from OPLS-DA and S plots) exhibited reasonable separation among the groups on the X-axis. The separation of various groups was also observed in the VIP score plots in Figs. 5 and 6, and the combined correlations of 2D OPLS-DA and the VIP score analysis exhibited significant differences in metabolic profiles among various groups. The various metabolites were carefully chosen when the statistically major threshold of variable influence on projection (VIP) values obtained from the OPLS-DA model was greater than 1.0. Moreover, the *p*-values from a two-tailed Student's t-test on the regulated peak area were considered statistically significant ($p < 0.05$). Log2-fold change (FC) was applied to demonstrate how these particularly differential metabolites varied among all the groups studied. The results were considered statistically significant when the p-value was less than 0.05.

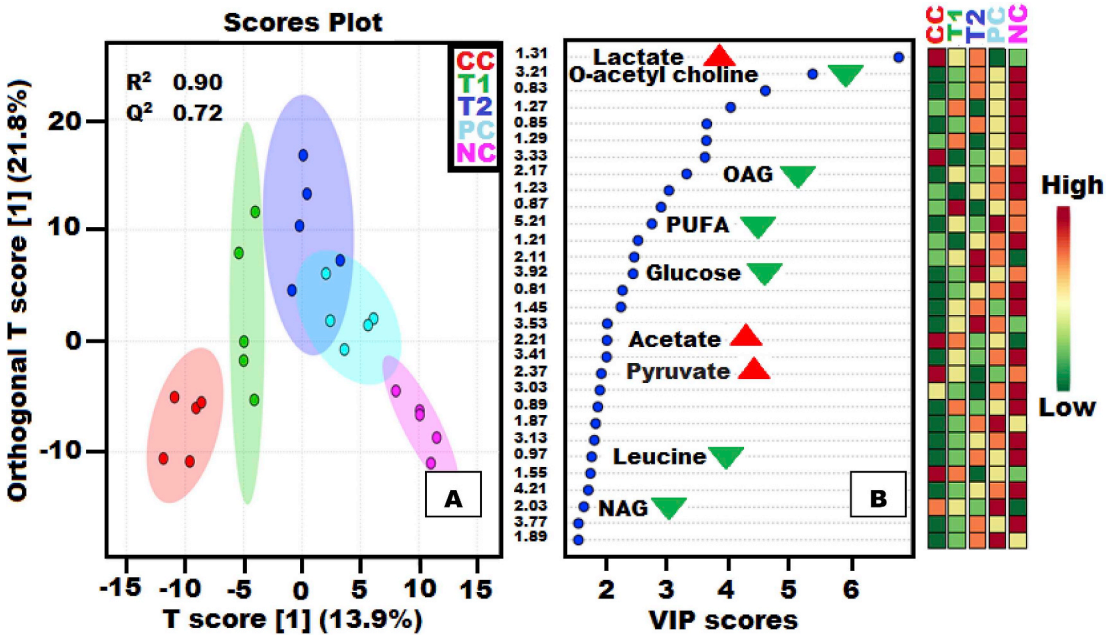


**Fig. 5.** Combined and Pairwise OPLS-DA analysis:(A)The 2D OPLS-DA analysis of 1D $^{1}$H CPMG NMR spectra score plot derived from combined analysis comprising of all the groups: Carcinogen control (CC), Treatment low dose (T1) & Treatment high dose (T2), Positive control (PC), Normal Control (NC). (B) The potential discriminatorymetabolite entities identified from VIP scores derived from PLS-DA modelling of complete data matrix and resulted VIP scores for top 30 metabolite entities are shown in increasing order of VIP score values to highlight their discriminatory potential.

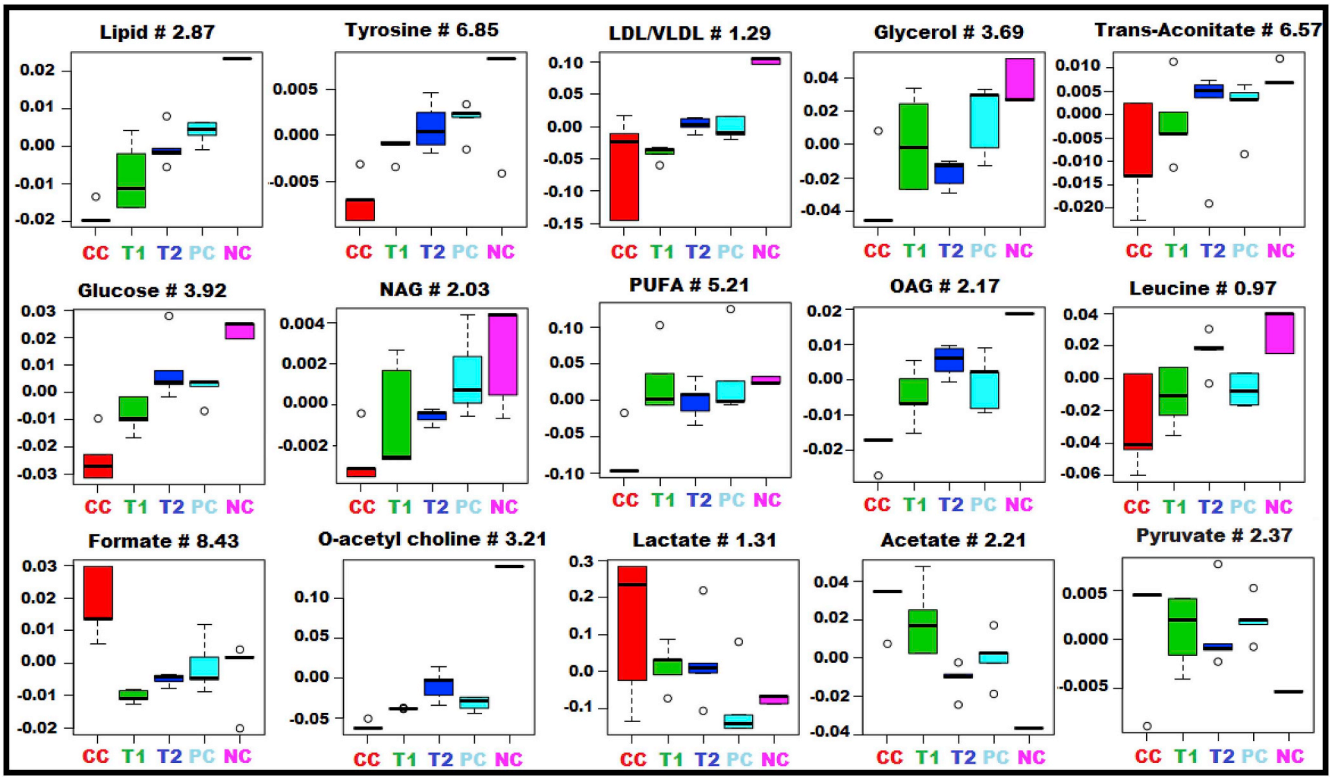


**Fig. 6.** Metabolic effects of zafirlukast treatment: The box-cum-whisker plots are showing relative variations in quantitative profiles of serum metabolites relevant in the context of the pathophysiology of hepatic cancer. In the box plots, the boxes denote interquartile ranges, horizontal line inside the box denote the median, and bottom and top boundaries of boxes are 25th and 75th percentiles, respectively. Lower and upper whiskers are 5th and 95th percentiles, respectively. Where: Carcinogen control (CC), Treatment low dose (T1) & Treatment high dose (T2), Positive control (PC), Normal Control (NC) groups.

Some relevant metabolic changes are shown in the form of univariate box plots in Figs. 5 and 6.

## 4. Discussion

The liver plays a vital role in various biochemical and physiological actions in the human body, and for the body to be healthy, the liver should always function properly. HCC has been the third most common cause of cancer-related death worldwide in the past five years (Ferlay et al., 2010; Lin et al., 2016), but chemotherapy against HCC is limited due to systemic toxicities and various side effects (Anadol et al., 2012). Sorafenib is the only FDA-approved drug for HCC, but it has a poor efficacy and systemic side effects (Park, 2015; Wilhelm et al., 2006). Currently, scientific communities are very prone to exploring new drug entities for HCC treatment. Consequently, we assumed that ZAF, since it is structurally similar to montelukast and exhibits CysLT1 antagonistic properties (Kahnt et al., 2013), might be a better alternative for HCC treatment. To determine the effects, we verified the anti-HCC properties of ZAF using Hep-G2 cells *in vitro* and found that ZAF had antineoplastic effects with an $IC_{50}$ ~13.95 μM. These data inspired us to perform *in vivo* antitumor activity experiments in a DEN-induced HCC rat model, after which we assembled a few notable findings that helped us explore the mechanisms underlying ZAF action in cancer therapy. Despite the availability of a few studies that reported the remarkable function of ZAF (as a CysLT1 antagonist) in a variety of activities including a protective role in breast cancer cells, to the best of our knowledge, none of the previously published studies revealed the role of ZAF inthe inhibition of HCC through this particular apoptotic pathway.

5-fluorouracil (5-FU) is an antimetabolic agent that is used to treat colorectal and liver cancer in combination. 5-FU exerts its anticancer effects through inhibition of thymidylate synthase and incorporation of its metabolites into RNA and DNA. Clinical efficacy of this drug is very low due to rapid acquired resistance (Longley et al., 2003), and therefore, identification of novel derivatives with different mechanisms for HCC treatment is a greater priority for the scientific community. In this regard, we explored the anticancer potential of ZAF through its activation of caspase-mediated apoptosis, i.e.i–NOS– and e–N-OS–mediated activation of Bcl-2 family proteins→CytC→Caspase 3 and 9 signaling cascade. On the contrary, a recent investigation suggested that ZAF exerts agonistic action on the CysLT receptor via changes in Bcl-2/BAX levels in glioblastoma (Piromkraipak et al., 2018).

DEN-treated rats showed a decrease in body weight, an increase in liver weight and a higher number of carcinogenic nodules, which indicates a carcinogenic condition. The normalization of these parameters after 5-FU and ZAF (80 mg/kg) treatments were the primary indication of the antineoplastic properties of ZAF, which led to further biochemical and histopathological analyses to demonstrate our hypothesis. A previous report suggested that antioxidant activity was decreased in carcinogenic conditions (Kweon et al., 2003). Reactive oxygen species (ROS) are generated from all aerobic cells and are counter balanced by an antioxidant defense system (Sharma et al., 2012). However, this action is unbalanced during hypoxic/anaerobic conditions such as cancer (due to excessive cellular proliferation) (Bhattacharyya et al., 2014). Actually, SOD and CAT are free radical scavengers, while GSH engulfs reactive oxygen species (ROS); together, these comprise the antioxidant defense mechanism of the human body (Shah et al., 2014). The concentrations of SOD, CAT and GSH were decreased, which indicates high cellular proliferation, in DEN-treated rats. The protective action of ZAF was observed when all these parameters were increased in the treatment groups. In general, the enzyme catalase (CAT) catalyzes the conversion of $H_2O_2$ to oxygen and water, thereby providing protection against reactive oxygen species, while SOD neutralizes superoxide free radicals (Karaman et al., 2006). Furthermore, oxidation of proteins and lipids can be characterized through higher production of

MDA and PC, respectively, and has been very well documented after DEN treatment (Kumar et al., 2017). The antioxidant defense mechanism of ZAF was again observed through reduced production of MDA and PC in treated rats, substantiating its ability to protect against tumors with notable antioxidant effects.

Furthermore, it has been shown that a corresponding change in GSH (reduced glutathione) and GSSG (oxidized glutathione) concentration is considered an actual sign of oxidative stress. If cells are under oxidative stress, GSSG accumulates and the ratio of GSH to GSSG generally decreases. Thus, the GSH/GSSG ratio is a strong indication of oxidative stress in liver cells. We therefore measured the GSG/GSSG ratio to analyze how much GSH was oxidized upon treatment with ZAF. In our experiment, the ZAF-treated group demonstrated an increase in the GSH/GSSG ratio, which indicates sustainment of inherent antioxidant properties by ZAF.

In addition, tumor-induced hyperlipidemia contributes to liver cirrhosis during HCC, which ultimately leads to liver damage (Huang et al., 2016). Liver damage during carcinogenesis was observed through increased TC, TG, LDL, and VLDL and decreased HDL concentrations in CC rat sera compared with NC rat sera. ZAF treatment normalized these concentrations, and the protective action of ZAF was further demonstrated in a similar experiment. In contrast, elevation of ALT and AST levels in the serum is an indication of liver cirrhosis (Green and Steven, 2002). ALP is another indicator of liver damage, and a high level of ALP is indicative of the high risk of HCC patients (Yu et al., 2011). Henceforth, in HCC and various pathological conditions, the liver becomes damaged, and various enzymes (AST, ALT and ALP) leak from the liver, which causes their levels in the blood stream to increase. Through the observed efficacy of ZAF in the restoration of these enzymes to normal levels, we determined the protective ability of ZAF. Similarly, an increase in serum LDH shows a nonspecific alteration of cell membrane integrity and liver cirrhosis in HCC (Xu et al., 2014). Therefore, higher levels of LDH in CC rat sera indicated DEN-induced HCC; the levels of LDH were further restored by ZAF administration. Further, elevated levels of catabolic by-products (bilirubin and biliverdin) also indicate liver disease (Makos and John, 1988). The elevation of these markers during DEN exposure and their normalization after ZAF treatment also supported the finding of hepatic disease control. Overall, ZAF has a protective ability to normalize these enzymes and their catabolic by-products, which demonstrates its antineoplastic properties against HCC. Furthermore, histopathological studies revealed that CC rats exhibited vacuole formation and irregularly shaped nuclei and cytoplasm, which was probably due to the generation of free radicals during DEN exposure. This vacuole formation was reduced in the ZAF and 5-FU groups, which demonstrates the protective ability of ZAF in cancerous conditions.

Then, we sought to determine the underlying mechanism of the antineoplastic properties of ZAF. ELISAs indicated that ZAF had no action on pro-inflammatory cytokines (IL-2, IL-6, IL-10 and IL-1β) but had positive action on apoptotic mediators (Caspase-3 and 9). In addition, it was necessary to evaluate the anti-HCC properties of ZAF at the molecular level. According to the preliminary data obtained from ELISAs, it is questionable whether ZAF had any effect on cellular apoptosis. Apoptosis occurs in two ways: the extrinsic death receptor pathway and the intrinsic mitochondrial pathway (Rang and Dale's Pharmacology, 2011). The Bcl-2 family proteins, including pro-apoptotic (BAX) and anti-apoptotic (Bcl-2) proteins are generated during the mitochondrial apoptosis pathway (Rang and Dale's Pharmacology, 2011). As per the qRT-PCR and Western blot results, we observed a lower expression of BAX and a higher expression of Bcl-2 in CC rats. The expression of these two proteins was normalized after ZAF treatment, which shows its ability to trigger mitochondrial apoptosis at the molecular level. This over expressed (i.e. BAX) protein binds to Cyt-C released from mitochondria, procaspase 9 and APAF1 to generate the apoptosome (Rang and Dale's Pharmacology, 2011). This apoptosome leads to apoptosis in the presence of caspases 3 and 9. qRT-PCR revealed that ZAF restored the decreased levels of caspases 3 and 9, and therefore, indicates that this drug is an important apoptosis activator. Altogether, these data show that ZAF may cause induction of apoptosis through i–NOS– and e–NOS–induced activation of Bcl-2 family proteins → Cy C → Caspase 3 and 9 signaling cascade.

The $^{1}$H-NMR-based metabolomics analysis provides a more discriminable signature and quantitative information of the metabolites in HCC before and after treatment (Frederich et al., 2016). The identification and characterization of perturbed metabolites in HCC may play a significant role in early diagnosis and therapy. This helps form a possible map for drug action in terms of the metabolomic pathways in HCC (Griffin and John, 2004). To the best of our knowledge, we report for the first time the impact of ZAF on HCC using $^{1}$H-NMR-based serum metabolomics. This analysis, coupled with multivariate statistical data analysis, investigated the DEN-induced metabolic alterations and assessed the ameliorative effect of ZAF treatment on these alterations. The HCC-associated metabolic pathway involves amino acids, ketone bodies, choline metabolism, glycolysis, the TCA cycle, phosphatidylinositol, and gluconeogenesis (Rahman and Hasan, 2015; Vander and Matthew, 2011).

In NMR-based metabolomic studies, we observed a decreased level of glucose and an increased level of lactate in CC rats compared with NC rats, which indicates an enhanced glycolytic pathway, and more glucose was consumed by cancerous cells with lactate as a by-product. This finding was similar to previously published observations of the Warburg effect (Asgari et al., 2015). The box and whisker plot showed lower levels of OAG, NAG and *O*-acetyl choline in CC rats. These are the important constituents of cell membranes in cancerous conditions, and therefore, decreased concentrations of these metabolites in CC rats were found in the NMR studies (Fages et al., 2015). It is obvious from the data that ZAF and 5-FU administration normalized the concentration of these metabolites, which demonstrates the protective ability of ZAF against HCC. Furthermore, decreased levels of VLDL and LDL were observed in the sera of rats in the CC group, as cholesterol, which is produced from both these metabolites, is utilized by cells for cell membrane production (Liu et al., 2014). ZAF administration normalized the concentrations of these metabolites to near normal levels, and thus evidence of the anticancer properties of ZAF was further strengthened.

Amino acids such as leucine and tyrosine are consumed by HCC cells during membrane formation, and maturation of cellular constituents occurs through these amino acids (Gao et al., 2009). We found depleted levels of these metabolites in the sera of HCC rats, as they were consumed at a higher rate by HCC tissues. In contrast, these metabolites were elevated in the 5-FU- and ZAF-treated rats. We again found a lower amount of glycerol in the serum of HCC rats, which demonstrates increased lipid metabolism in cancer (Rahman and Hasan, 2015; Vander and Matthew, 2011). Treatment with 5-FU and ZAF normalized the level of glycerol in the serum, which indicates the ability of these compounds to enhance glycerol metabolism. In addition, ZAF treatment also normalized trans-aconitate, pyruvate, formate and acetatein the serum, and the protective action of ZAF was observed in a similar experiment.

## 5. Conclusion

The discovery of a novel drug for HCC treatment has been very difficult since the molecular mechanism of HCC is still unknown. According to the current demands of HCC treatment, we proposed a cellular function for ZAF in HCC treatment at the molecular level. The current study supported a clear link among biochemical, pathophysiological, molecular and metabolic parameters after treatment with 5-FU and ZAF. The molecular insights observed in this study could explain the role of ZAF in HCC treatment as occurring through the suppression of Bcl-2 and upstream regulation of BAX proteins, i.e. the activation of caspase-mediated mitochondrial apoptosis. The combined analysis of

gene and protein expression revealed that ZAF has the potential to induce apoptosis through i–NOS– and e–NOS–induced activation of the Bcl-2 family of proteins→CytC→Caspase 3 and 9 signaling cascade. Finally, an $^{1}$H-NMR-based metabolomics approach clearly discriminated the regulation of advanced metabolites in HCC and after ZAF treatment, which could demonstrate the cellular function of ZAF. Altogether, ZAF may be an alternative for HCC treatment from a future drug design perspective.

## Declaration of competing interest

The authors declare that they have no known competing financial interests or personal relationships that could have appeared to influence the work reported in this paper.

## Acknowledgements

Dr. Sudipta Saha would like to thank to UGC, India, for MRP grant [Project no. 42-680/2013(SR)] and DST, India for SERB project (Ref. No. DST/SB/EMEQ-320/2014). The authors also express their sincere gratitude to CBMR, Lucknow for providing the NMR facilities. Mr. Pranesh Kumar acknowledged DST India for the INSPIRE Fellowship (DST/INSPIRE Fellowship/2016/IF160364).

## Appendix A. Supplementary data

Supplementary data to this article can be found online at https://doi.org/10.1016/j.yrtph.2019.104489.

## References

Anadol, E., et al., 2012. The changes of inducible nitric oxide synthase, endothelial nitric oxide synthase and cyclooxygenase-2 mRNA expressions in intrauterine tissues of pregnant rats. Ankara Univ. Vet. Fak. Derg. 59, 295–301.
Asgari, Y., et al., 2015. Alterations in cancer cell metabolism: the Warburg effect and metabolic adaptation. Genomics 105, 275–281.
Bhattacharyya, A., et al., 2014. Oxidative stress: an essential factor in the pathogenesis of gastrointestinal mucosal diseases. Physiol. Rev. 94, 329–354.
Chandra, D., et al., 2002. Early mitochondrial activation and cytochrome c up-regulation during apoptosis. J. Biol. Chem. 277, 50842–50854.
Frederich, M., et al., 2016. Metabolomics as a challenging approach for medicinal chemistry and personalized medicine. J. Med. Chem. 59, 8649–8666.
Ferlay, J., et al., 2010. Estimates of worldwide burden of cancer in 2008: globocan 2008. Int. J. Cancer 127, 2893–2917.
Fages, A., et al., 2015. Metabolomic profiles of hepatocellular carcinoma in a European prospective cohort. BMC Med. 13, 1–14.
Green, R.M., Steven, F., 2002. AGA technical review on the evaluation of liver chemistry tests. Gastroenterology 123, 1367–1384.
Gao, H., et al., 2009. Application of 1H NMR-based metabonomics in the study of metabolic profiling of human hepatocellular carcinoma and liver cirrhosis. Cancer Sci. 100, 782–785.
Griffin, J.L., John, P.S., 2004. Metabolic profiles of cancer cells. Nat. Rev. Cancer 4, 551.
Huang, J., et al., 2016. Tumor-induced hyperlipidemia contributes to tumor growth. Cell Rep. 15, 336–348.
Han, S., et al., 2016. Ginsenoside 20 (S)-Rh2 exerts anti-cancer activity through targeting IL-6-induced JAK2/STAT3 pathway in human colorectal cancer cells. J. Ethnopharmacol. 194, 83–90.
Jafari, A.I., et al., 2008. Evaluation of Bcl-2 family gene expression and Caspase-3 activity in hippocampus STZ-induced diabetic rats. Exp. Diabetes Res. 1–6.
Karaman, A., et al., 2006. Hepatic damage in biliary-obstructed rats is ameliorated by leflunomide treatment. Pediatr. Surg. Int. 22, 701–708.
Keshari, A.K., et al., 2017. 5H-benzo [h] thiazolo [2, 3-b] quinazolines ameliorate NDEA-induced hepatocellular carcinogenesis in rats through IL-6 downregulation along with oxidative and metabolic stress reduction. Drug Des. Dev. Ther. 11, 2981–2995.
Kumar, A., et al., 2015. Silibinin inhibits the hepatocellular carcinoma in NDEA-induced rodent carcinogenesis model: an evaluation through biochemical and bio-structural parameters. J. Cancer Sci. Ther. 7, 206–215.
Kahnt, A.S., et al., 2013. Cysteinyl leukotriene-receptor-1 antagonists interfere with PGE2 synthesis by inhibiting mPGES-1 activity. Biochem. Pharmacol. 86, 286–296.
Kweon, S., et al., 2003. Chemopreventive effect of garlic powder diet in diethylnitrosamine-induced rat hepatocarcinogenesis. Life Sci. 73, 2515–2526.
Kumar, P., et al., 2017. 6, 7-dimethoxy-1, 2, 3, 4-tetrahydro-isoquinoline-3-carboxylic acid attenuates heptatocellular carcinoma in rats with NMR-based metabolic perturbations. Future Sci. OA 3 (FSO202), 1–18.
Kumar, P., et al., 2018. Poly (lactic-co-glycolic acid)-loaded nanoparticles of betulinic acid for improved treatment of hepatic cancer: characterization, in vitro and in vivo evaluations. Int. J. Nanomed. 13, 975–990.
Liu, Y., et al., 2014. NMR and LC/MS-based global metabolomics to identify serum biomarkers differentiating hepatocellular carcinoma from liver cirrhosis. Int. J. Cancer 135, 658–668.
Lin, J., et al., 2016. Combination treatment including targeted therapy for advanced hepatocellular carcinoma. Oncotarget 7, 71036–71051.
Longley, D.B., et al., 2003. 5-fluorouracil: mechanisms of action and clinical strategies. Nat. Rev. Cancer 3, 330–338.
Mahgoub, A.A., et al., 2003. Evaluating the prophylactic potential of zafirlukast against the toxic effects of acetic acid on the rat colon. Toxicol. Lett. 145, 79–87.
Makos, B.K., John, H.Y., 1988. Tissue levels of bilirubin and biliverdin in the sea lamprey, Petromyzon marinus L., before and after biliary atresia. Comp. Biochem. Physiol. C Toxicol. Pharmacol. 91, 701–710.
Matsuzaki, T., et al., 1992. Liver transplantation for diethylnitrosamine-induced hepatocellular carcinoma in rats. Transplant. Proc. 24, 748–751.
Osman, J., et al., 2017. Cysteinyl leukotriene receptor 1 facilitates tumorigenesis in a mouse model of colitis-associated colon cancer. Oncotarget 8, 34773–34786.
Park, J.G., 2015. Long-term outcomes of patients with advanced hepatocellular carcinoma who achieved complete remission after sorafenib therapy. Clin. Mol. Hepatol. 21, 287–294.
Piromkraipak, P., et al., 2018. Cysteinyl leukotriene receptor antagonists induce apoptosis and inhibit proliferation of human glioblastoma cells by downregulating B-cell lymphoma 2 and inducing cell cycle arrest. Can. J. Physiol. Pharmacol. 96, 798–806.
Rang, Dale's Pharmacology, 2011. 7th Edition, Publisher: Churchill Livingstone.
Rahman, M., Hasan, M.R., 2015. Cancer metabolism and drug resistance. Metabolites 5, 571–600.
Savari, S., et al., 2013. CysLT1R antagonists inhibit tumor growth in a xenograft model of colon cancer. PLoS One 8, 1–14 e73466.
Sharma, P., et al., 2012. Reactive oxygen species, oxidative damage, and antioxidative defense mechanism in plants under stressful conditions. J. Bot., Le 26 Article ID 217037.
Shah, D., et al., 2014. Oxidative stress and its biomarkers in systemic lupus erythematosus. J. Biomed. Sci. 21, 23.
Sahdev, A.K., et al., 2017. Ameliorative effects of pyrazinoic acid against oxidative and metabolic stress manifested in rats with dimethylhydrazine induced colonic carcinoma. Canc. Boil. Ther. 18, 304–313.
Singh, A.K., et al., 2018a. Novel Indole-fused benzo-oxazepines (IFBOs) inhibit invasion of hepatocellular carcinoma by targeting IL-6 mediated JAK2/STAT3 oncogenic signals. Sci. Rep. 8, 1–13.
Singh, A.K., et al., 2018b. Isolated mangiferin and naringenin exert antidiabetic effect via PPARγ/GLUT4 dual agonistic action with strong metabolic regulation. Chem. Boil. Interact. 280, 33–44.
Sui, H., et al., 2011. COX-2 contributes to P-glycoprotein-mediated multidrug resistance via phosphorylation of c-Jun at Ser63/73 in colorectal cancer. Carcinogenesis 32, 667–675.
Ulrich, E.L., et al., 2007. BioMagResBank. Nucleic Acids Res. 36, D402–D408.
Vander, H., Matthew, G., 2011. Targeting cancer metabolism: a therapeutic window opens. Nat. Rev. Drug Discov. 10, 671–684.
Wishart, D.S., et al., 2007. HMDB: the human metabolome database. Nucleic Acids Res. 35, D521–D526.
Wilhelm, S., et al., 2006. Discovery and development of sorafenib: a multikinase inhibitor for treating cancer. Nat. Rev. Drug Discov. 5, 835–844.
Xia, J., et al., 2009. MetaboAnalyst: a web server for metabolomic data analysis and interpretation. Nucleic Acids Res. 37, W652–W660.
Xia, J., et al., 2015. MetaboAnalyst 3.0—making metabolomics more meaningful. Nucleic Acids Res. 43, W251–W257.
Xu, W., et al., 2016. Activation of Bcl-2-caspase-9 apoptosis pathway in the testis of asthmatic mice. PLoS One 11, e0149353.
Xu, H.N., et al., 2014. Is higher lactate an indicator of tumor metastatic risk? A pilot MRS study using hyperpolarized 13C-pyruvate. Acad. Radiol. 21, 223–231.
Yadav, R.K., et al., 2015. Cytotoxicity of different extracts of Mucuna pruriens seeds on hepatoma cells but not on normal hepatic cells. Pharmacogn. Commun. 5, 63–69.
Yu, M.C., et al., 2011. Alkaline phosphatase: does it have a role in predicting hepatocellular carcinoma recurrence? J. Gastrointest. Surg. 15, 1440–1449.